Supporting Information

Definition of Redox Centers in Reactions of Lithium Intercalation in Li_3RuO_4 Polymorphs

Haifeng Li,[†] Srinivasan Ramakrishnan,[‡] John W. Freeland,[§] Bryan D. McCloskey,[‡] Jordi Cabana*,[†]

[†]Department of Chemistry, University of Illinois at Chicago, Chicago, Illinois 60607, United States

[‡]Department of Chemical and Biomolecular Engineering, University of California, Berkeley, California 94720, United States

[§]Advanced Photon Source, Argonne National Laboratory, Lemont, Illinois 60439, United States

*Corresponding email: jcabana@uic.edu

Contents

EXPERIMENTAL DETAILS

Sample Preparation

Two polymorphs of Li_3RuO_4 were prepared through a traditional solid-state reaction from mixtures of RuO_2 (Sigma-Aldrich, 99.9%) with a 10% stoichiometric excess of Li_2O (Sigma-Aldrich, 99.9%). The reactants were mixed in an agate mortar and pestle before grinding in a planetary ball mill using a zirconia set for 1 h at 500 rpm and then the homogeneous mixture was compacted into pellets. The pellets were reacted at either 650℃ or 900℃ for 24 hours in an alumina crucible under air, respectively. After cooling to room temperature naturally, the as-obtained polymorph samples were ground into fine powders.

Sample Characterization

Crystal structure analysis

Ex situ diffraction: Laboratory powder X-ray diffraction (pXRD) profiles were collected by scanning from 10° to 90°, 2θ, using a step size of 0.019°, at a rate of 2.6×10^{-5} °/min 2θ, in a custom air-free sample holder, in a Bruker D8 Advance diffractometer operating at 40 kV and 40 mA with Cu Kα radiation (λ = 1.5418 Å). Synchrotron X-ray diffraction measurements (SXRD) were recorded at the 11-BM beamline of the Advanced Photon Source (APS) at Argonne National Laboratory. An appropriate amount of amorphous silicon dioxide was introduced and mixed homogeneously with sample powders to reduce X-ray absorption and subsequently to increase the ratio of intensity to background. The powders were sealed in Kapton capillaries with a diameter of 0.8 mm. Air-sensitive samples were loaded and sealed under Ar in a glove box to minimize the exposure to ambient O_2. Time of flight neutron powder diffraction (TOF-NPD) data were collected at room temperature at the beamline 11A (POWGEN) of the Spallation Neutron Source (SNS) at

Oak Ridge National Laboratory (ORNL) with the center wavelength of neutrons of 1.5 Å. An appropriate amount of samples were sealed in airtight vanadium sample cans with the inner diameter of 6 mm under argon and transferred to the beamline station. The Rietveld refinements were performed using GSASII.[1]

Operando X-ray diffraction: The electrode was prepared by mixing 60 wt% D-Li_3RuO_4, 10 wt% carbon black (Vulcan XC-72, Cabot Corporation), 10 wt% Super P carbon (Alfa Asear), 20 wt% polytetrafluoroethylene (PTFE) (Sigma-Aldrich) in a mortar and pestle in an argon-filled glovebox. The homogeneous mixture powder was pressed into an 11 mm diameter pellet with a thickness of ~150 μm and a mass of ~20 mg. The AMPIX[2] cell was assembled in the argon-filled glovebox using Li metal as the counter electrode, a Whatman GF/B borosilicate microfiber filter as the separator, and 1 M solution of $LiPF_6$ in a 1:1 mixture of ethylene carbonate (EC)/dimethyl carbonate (DMC) as the electrolyte (Tomiyama Pure Chemical Industries).

Operando SXRD experiments were performed at high-energy beamlines 17-BM (λ = 0.25463 Å) and 11-ID-B (λ = 0.2113 Å) of APS at Argonne National Laboratory to collect data of D-Li_3RuO_4 cycled within the voltage window of 2.5-3.9 V and 1.5-2.5 V, respectively. A room temperature galvanostatic charge/discharge experiment was carried out with a cycler (Maccor model 4300) at C/10 (indicating 1 equivalent Li is extracted in 10 h) within the specified cutoff window. Diffraction images were recorded in a Debye–Scherrer geometry using an amorphous silicon-based area detector with time interval of 10 mins at 17-BM-B and 30 mins at 11-ID-B. The data were calibrated using GSAS-II software via LaB_6 calibrant (SRM660a) for 17-BM-B data and using a CeO_2 standard (SRM674b) for 11-ID-B data and integrated within GSAS-II.[1]

Scanning electron microscopy (SEM) was used to analyze the particle size and morphology of samples. Micrographs were collected on a Hitachi S-3000N microscope operated at 5 kV and 20 mA.

Electrochemical characterization

Galvanostatic experiments were carried out in two-electrode 2032 coin-type cells. Li_3RuO_4 was homogeneously mixed in a planetary ball mill for 1 h at 500 rpm with 10 wt% carbon black (Denka) under Argon atmosphere before further experiments. Working electrodes were prepared from the uniformly ballmilled mixtures, and 10 wt% polyvinylidene fluoride (PVDF) (Kynar) in 1-methyl-2-pyrrolidone (NMP, Sigma−Aldrich). The slurries were cast on an electrochemical grade aluminum foil using a doctor blade, followed by drying under vacuum at 110 °C overnight. Dried electrodes with typical active material loadings of 3-5 mg/cm^2 were punched into pieces with a diameter of ½ inch for further cell assembling. All the cells were fabricated in an argon-filled glovebox with moisture and oxygen levels of lower than 0.1 ppm. Within the cells, a high-purity lithium foil (Alfa Aesar) was employed as the counter/reference electrode, and a 25-μm-thick polypropylene membrane (Celgard 2400) was used as the separator, and a solution of 1 M $LiPF_6$ in a mixture of ethylene carbonate (EC)/dimethyl carbonate (DMC) (1:1, V/V, Novolyte Technologies) was employed as the electrolyte. The galvanostatic charge–discharge cycling was performed at room temperature using a BT-Lab tester with a current rate of C/10 (indicating 1 equivalent Li is extracted in 10 h) with different voltage-cutoff windows. All potentials quoted in this paper were referenced to Li^+/Li^0 unless otherwise mentioned. For *ex situ* experiments, when the state of the cell reached a point of chemical interest, it was stopped and immediately disassembled in the argon-filled glovebox to avoid self-discharging under open-circuit state. The

working electrode was washed with DMC three times followed by drying under vacuum inside the glove box antechamber for 5 mins.

X-ray Absorption Spectroscopy

Ex situ O K-edge X-ray absorption spectroscopy (XAS) measurements were performed at 4-ID-C beamline of APS at Argonne National Laboratory. Samples were attached to a copper sample holder using conductive carbon tape in an argon-filled glovebox and then transferred from the glovebox into a transport container and then into an X-ray absorption antechamber through an argon environment to minimize the potential exposure to air. Data were measured simultaneously under both the total electron yield (TEY) mode from the sample photocurrent at ~10^{-9} Torr and total fluorescence yield (TFY) mode using a silicon drift diode detector. The angle of X-ray incidence in TFY mode was adjusted to minimize the self-absorption while still being bulk sensitive. Data was obtained at a spectral resolution of ~0.2 eV, with a 2 s dwell time. During the measurement, three scans were performed at each absorption edge for each sample, and scans were then averaged to maximize the signal-to-noise ratio. The energy scale of the spectra was calibrated with a Sr_2RuO_4 reference measured simultaneously.

Ex situ Ru K-edge X-ray absorption near edge spectroscopy (XANES) data were collected under the transmission mode at the Materials Research Collaborative Access Team (MRCAT) Sector 10-BM beamline of the APS using an Oxford Si (111) double crystal monochromator with an energy resolution of 1.1 eV at 22 keV. Three consecutive ionization-chamber detectors were used to count the intensity of the monochromatic X-ray beam. Samples were placed between the first and second ionization chambers. Prior to the beam setup, the calibration for monochromic energy was established by measuring the Ru K-edge of a standard foil of Ru metal located between the second

and third ion-chamber. During the measurement, successive spectra were averaged out over periods of 5.5 min based on the scanning time of 0.3 s. The K-edge of the standard Ru foil was measured simultaneously with each sample for energy alignment. Pre-edge background subtraction and XANES normalization were carried out using the Demeter program pack with Athena.[3] All samples for Ru K-edge XANES were cut from the same working electrodes as for O K-edge XAS.

Differential Electrochemical Mass Spectrometry (DEMS)

The quantitative outgassing measurements were performed in a hermetically-sealed cell fitted with gas capillaries connected to a custom-built DEMS system described in detail in previous publications.[4-7] The cell was assembled with the as-prepared electrode as the working electrode, Li foil (11 mm diameter) as the counter electrode, one Celgard® 2400 film and one QMA (Whatman) glass fiber separators, each 12 mm in diameter. A 1 M solution of $LiPF_6$ (Sigma-Aldrich) in an ethylene carbonate (EC)–diethyl carbonate (DEC) solvent mixture (1:1, V/V, BASF) was employed as the electrolyte. Electrode preparation as well as cell fabrication were performed under air-free conditions in an argon-filled glovebox. The assembled cells were cycled with a Bio-Logic VSP series potentiostat at a rate of 0.1 Li^+/hour. During battery cycling, the headspace of our custom cell was sampled with argon as the carrier gas. The CO_2 and O_2 evolved were quantified based on calibrations of the mass analyzer with known amounts of CO_2 and O_2 with argon as the carrier gas.

The total active cathode material used for the measurement was 5.9 mg disordered Li_3RuO_4 (32 μmol) and ordered Li_3RuO_4 7.0 mg (38 μmol). Cells were cycled between 3.9 and 2.5 V for

disordered Li_3RuO_4 and between 4.0 and 2.5 V for ordered Li_3RuO_4, under the current of 14 mAg^{-1}.

SUPPLEMENTARY FIGURES

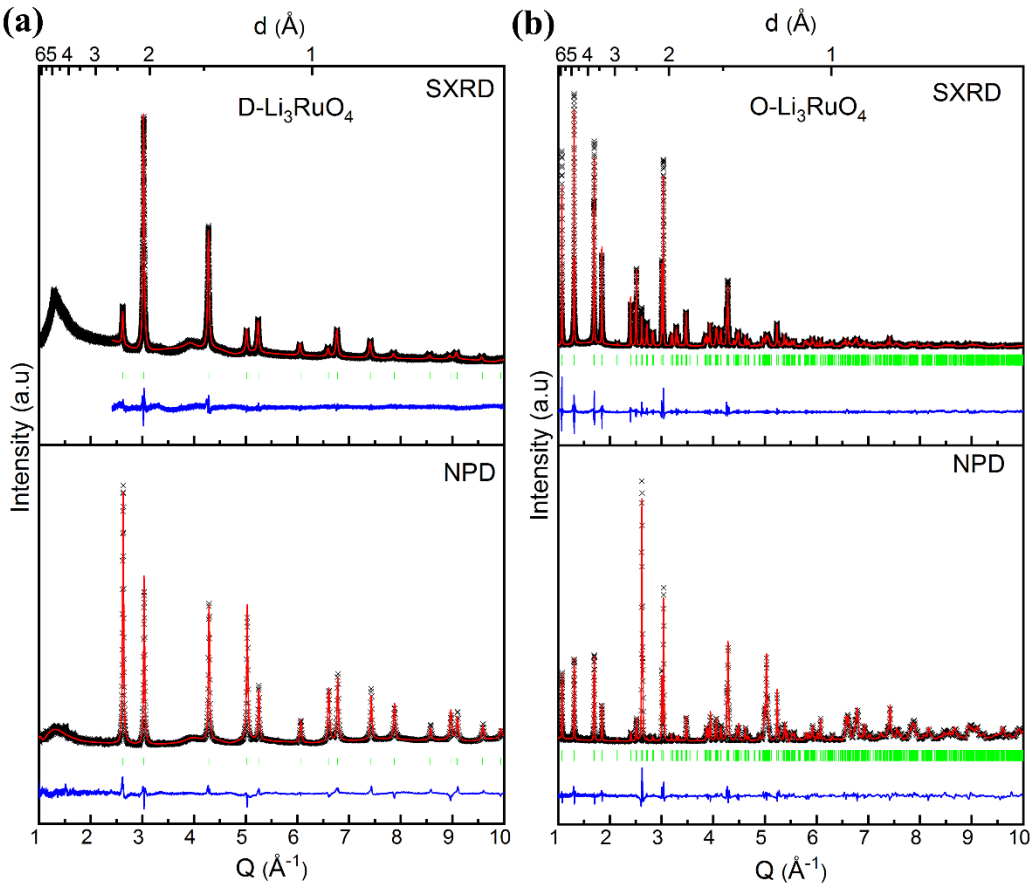

Figure S1. Structural characterization of disordered and ordered Li_3RuO_4. Combined Rietveld refinement of SXRD and NPD patterns of (a) D-Li_3RuO_4 and (b) O-Li_3RuO_4. Black crosses: experimental patterns, red solid line: calculated patterns, blue solid line: difference and green bars: Bragg reflections.

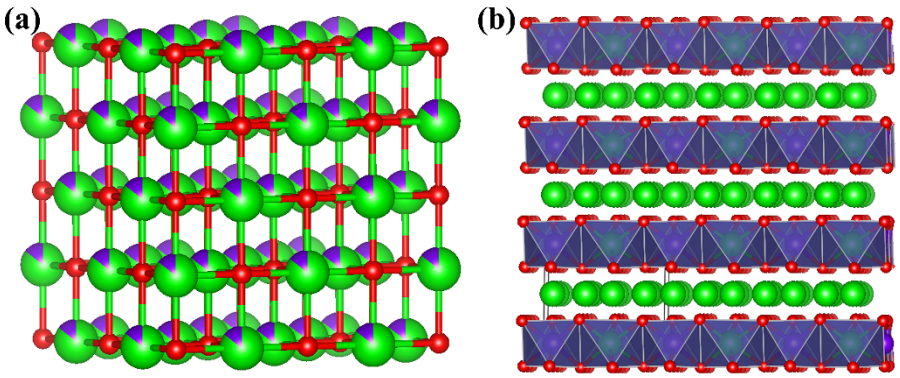

Figure S2. Structure of (a) D- and (B) O-Li_3RuO_4. Oxide ions (red) stack in a cubic close-packed arrangement while both Li (green) and Ru (purple) occupy octahedral sites for both polymorphs. D-Li_3RuO_4 has mixed Li and Ru arrangement in the metallic layers. O-Li_3RuO_4 has a long-range distribution of zig-zag chains.

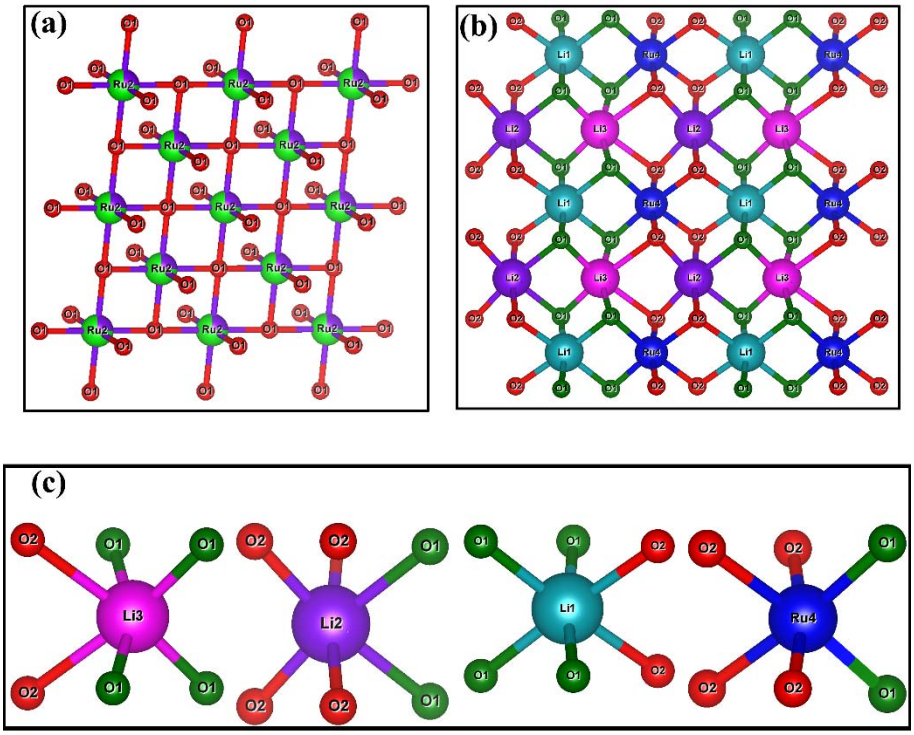

Figure S3. Schematic arrangement of various bonds in (a) D- and (b) O-Li_3RuO_4. (c) Individual coordination environment for each cation in O-Li_3RuO_4.

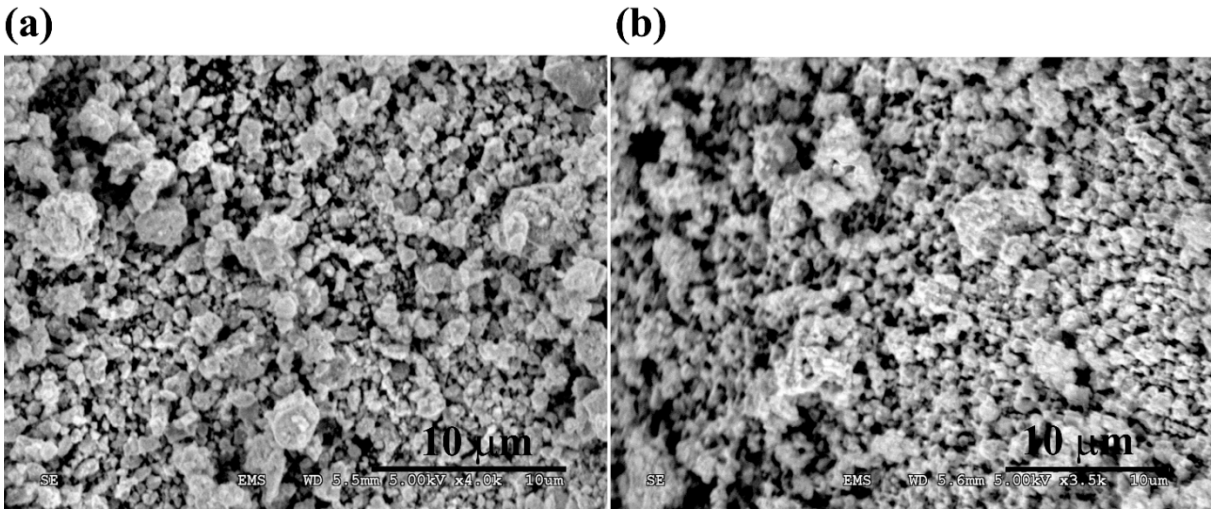

Figure S4. SEM images of (a) D- and (b) O-Li_3RuO_4.

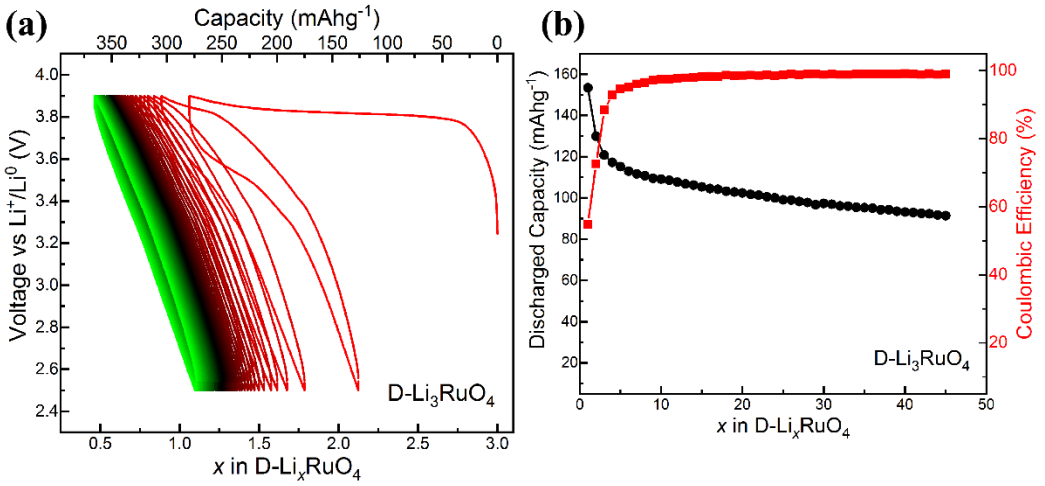

Figure S5. Voltage-composition profile of D-Li_3RuO_4 between 2.5 and 3.9 V upon extensive cycling; (b) Discharge capacity and coulombic efficiency as a function of the cycle number.

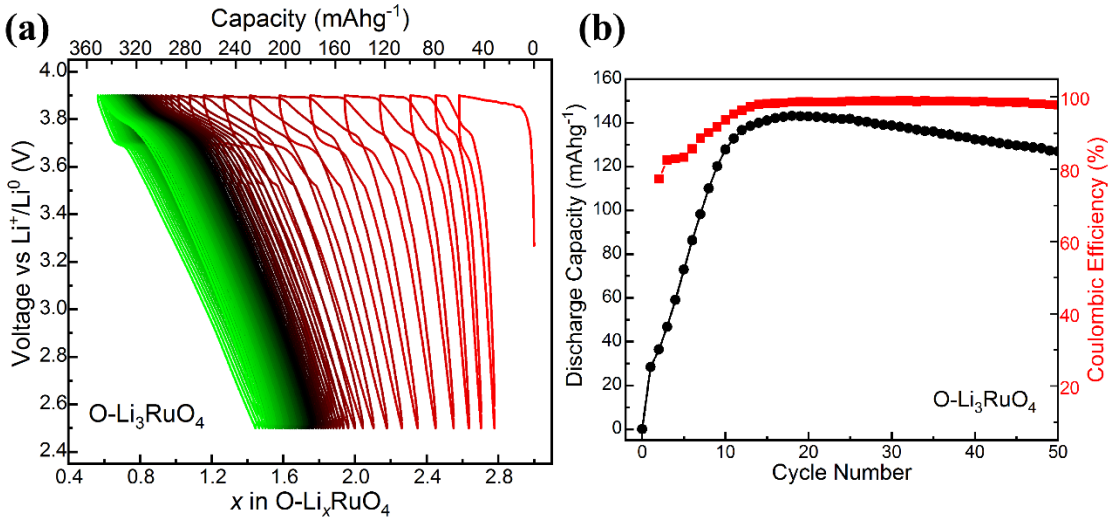

Figure S6. Voltage-composition profile of O-Li_3RuO_4 between 2.5 and 3.9 V upon extensive cycling; (b) Discharge capacity and coulombic efficiency as a function of the cycle number.

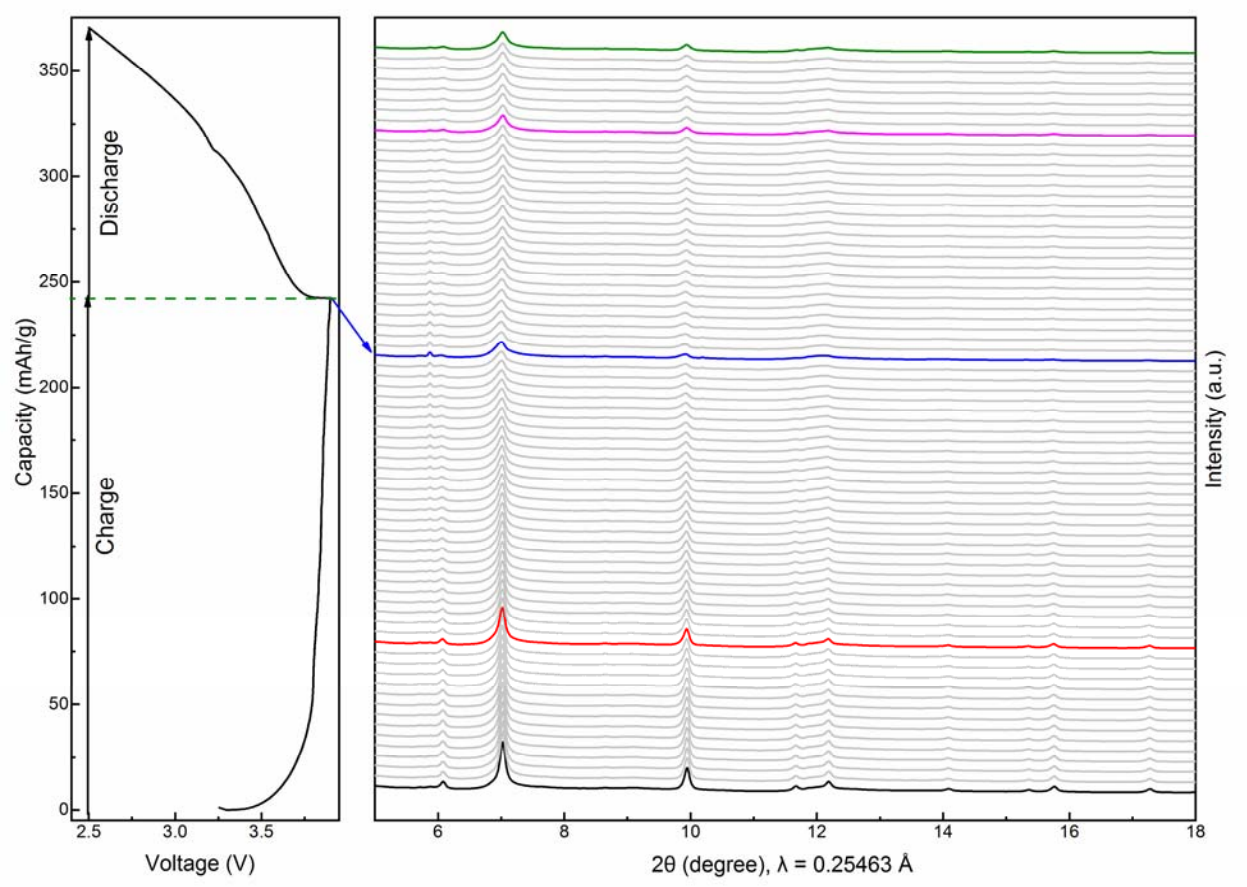

Figure S7. *Operando* SXRD patterns in the first cycle of a D-Li_3RuO_4/Li half-cell at a rate of C/20. The left panel shows the corresponding galvanostatic curve between 2.5 and 3.9 V. Colored lines indicate key points in the experiment, discussed in the text.

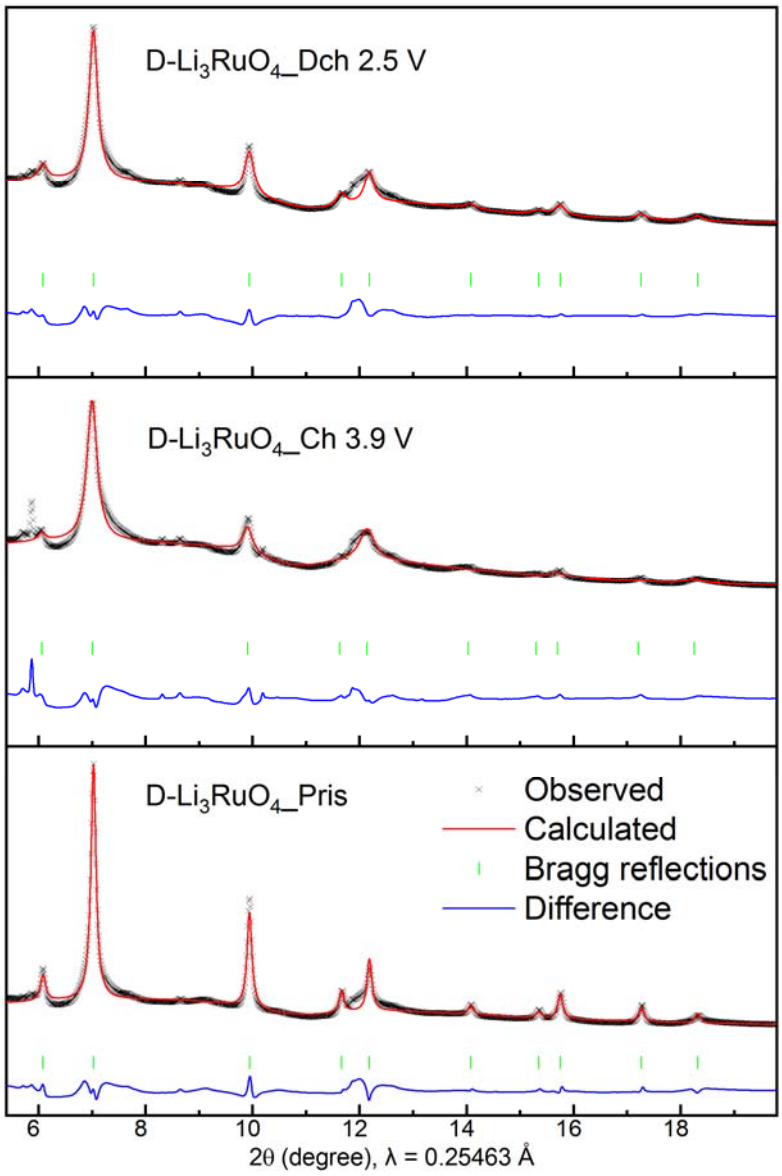

Figure S8. Pawley refinements of SXRD patterns of D-Li_3RuO_4 at different electrochemical states between 2.5 and 3.9 V.

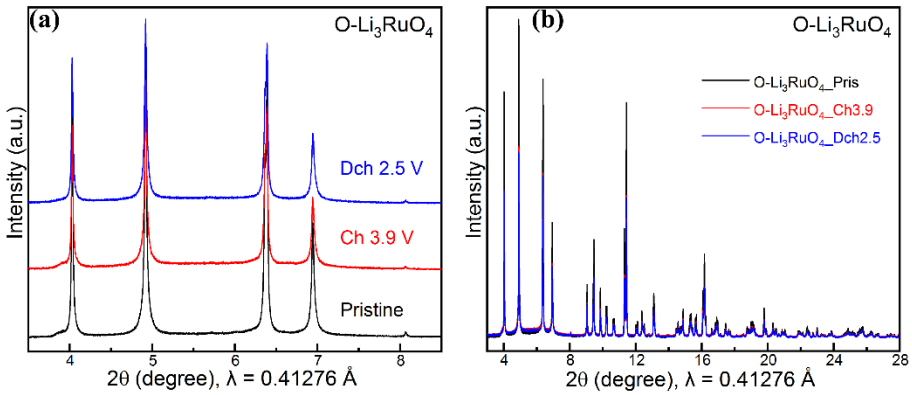

Figure S9. (a) Enlarged and (b) overlaid SXRD patterns of O-Li_3RuO_4 during the first cycle. There was no obvious peak shift upon cycling. The intensity experienced substantial decrease after oxidation to 3.9 V, while the subsequent reduction did not bring about remarkable change in the intensity in relative to that of the previous oxidation.

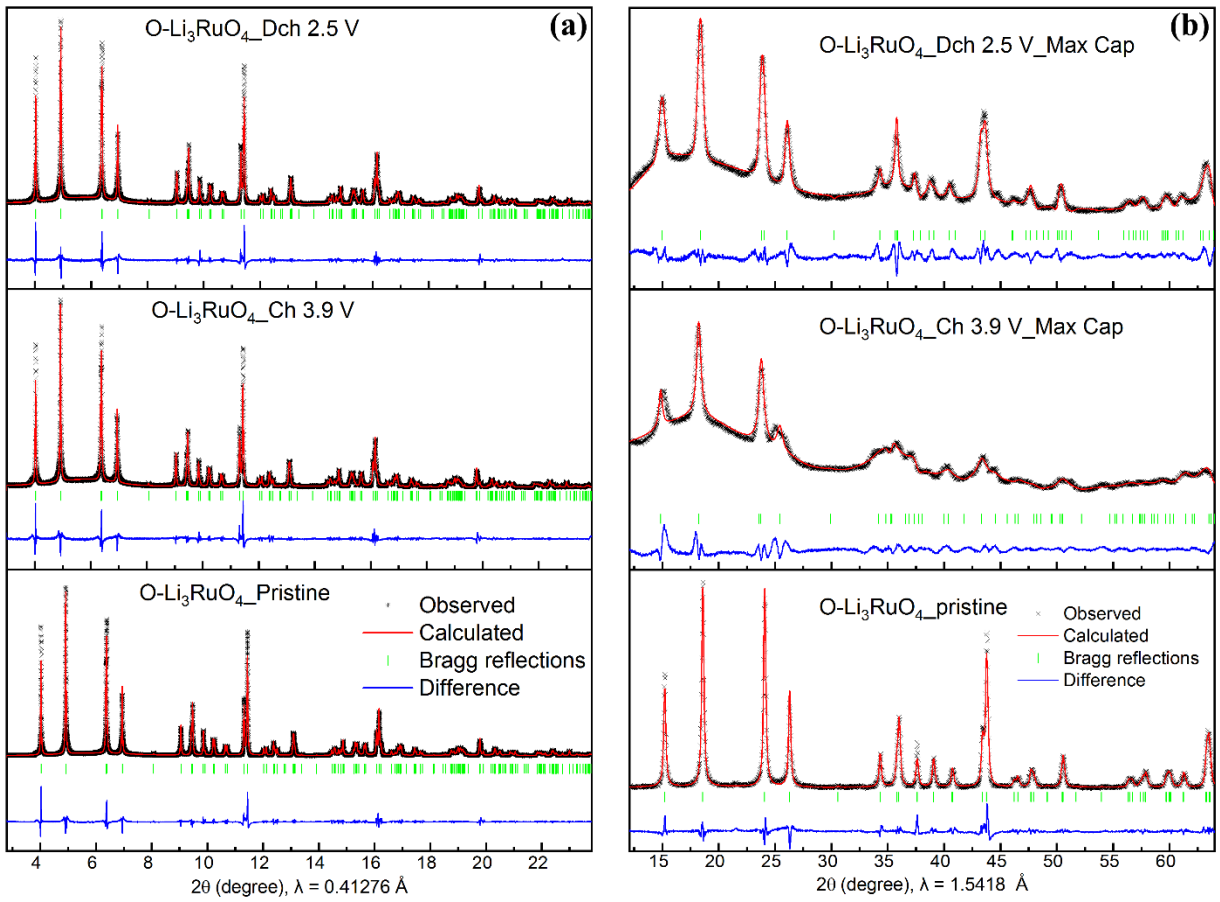

Figure S10. Pawley refinements of XRD patterns of O-Li_3RuO_4 at different electrochemical states. Panel a shows the SXRD patterns. Panel b portraits the XRD results collected by the Cu Kα irradiation.

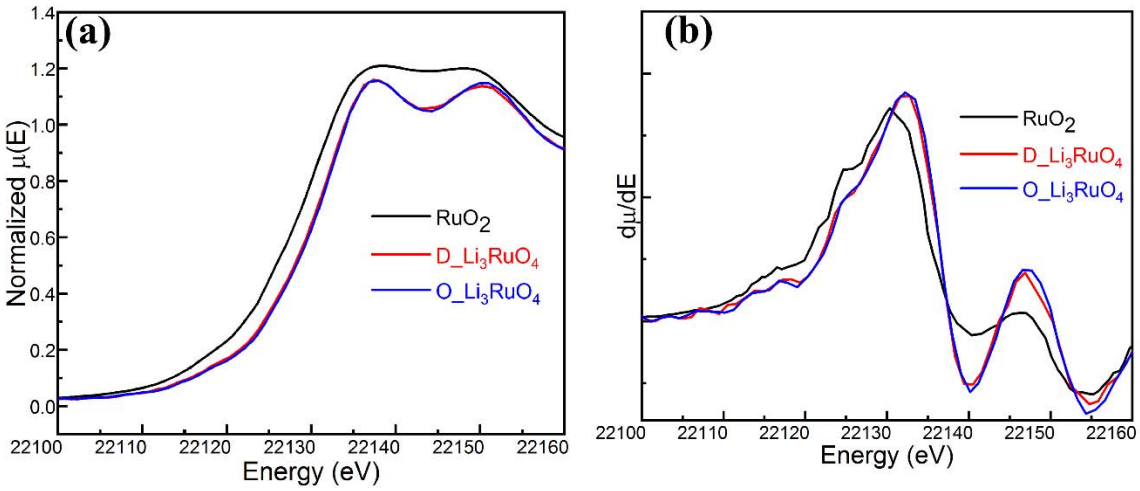

Figure S11. (a) *Ex situ* Ru K-edge XANES spectra and (b) the corresponding derivative curves of RuO_2, disordered Li_3RuO_4 and ordered Li_3RuO_4.

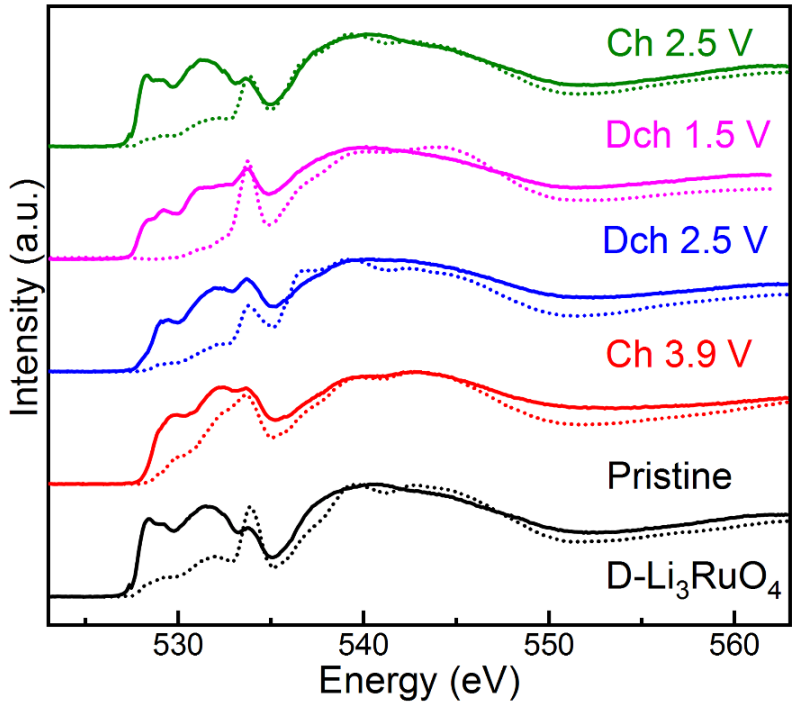

Figure S12. *Ex situ* O K-edge XAS spectra of disordered Li_3RuO_4 at different states collected under TEY (dot line) and TFY (solid line) detection modes.

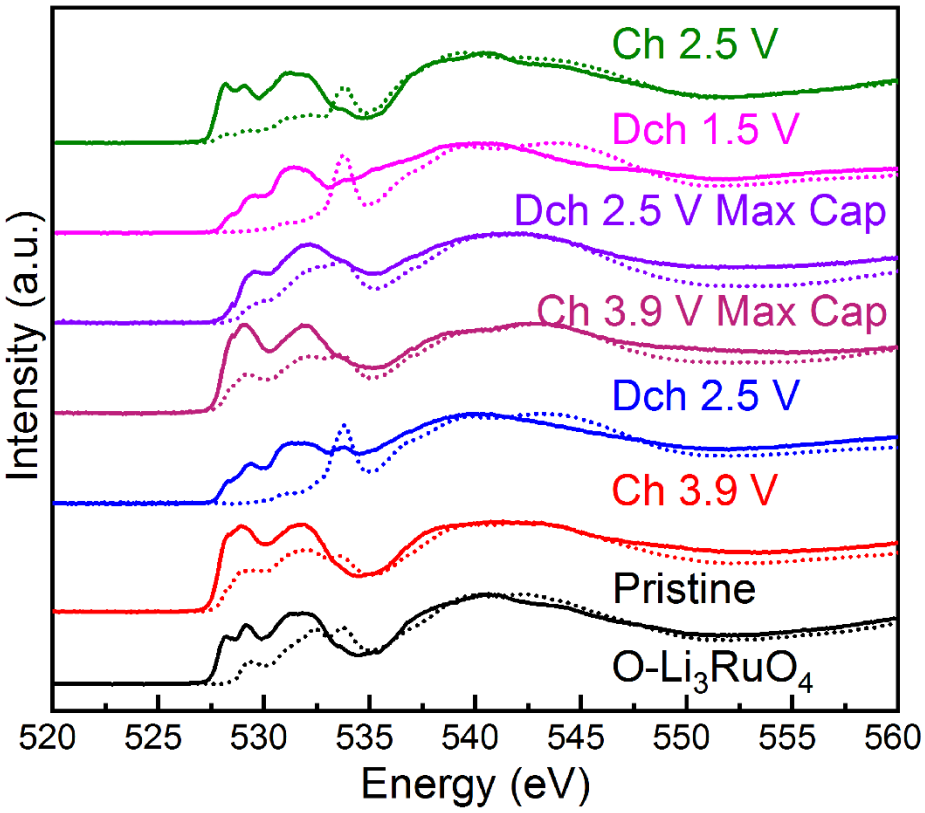

Figure S13. *Ex situ* O K-edge XAS spectra of ordered Li_3RuO_4 at different states collected under TEY (dot line) and TFY (solid line) detection modes.

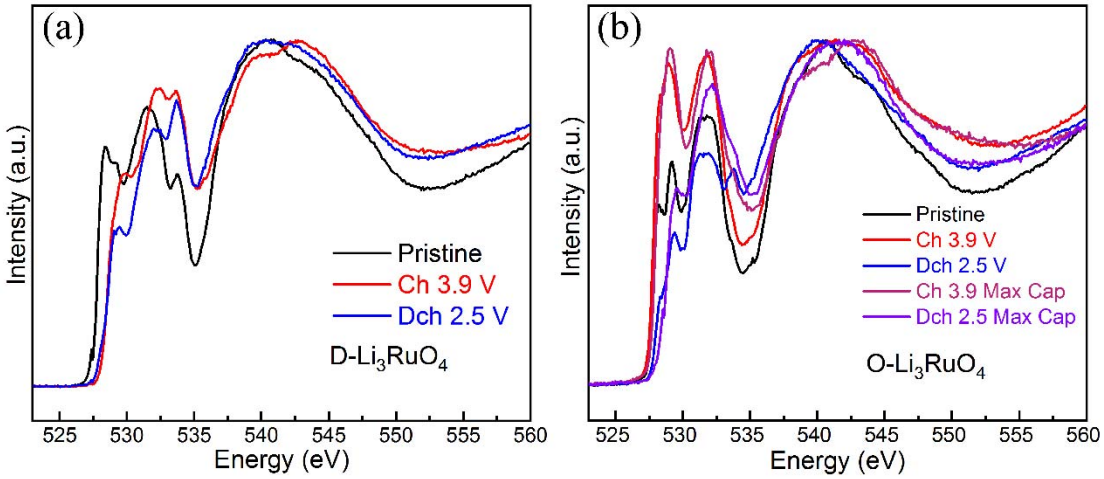

Figure S14. Overlaid *Ex situ* O K-edge XAS spectra of (a) D- and (b) O-Li_3RuO_4 measured at different electrochemical states between 2.5 and 3.9 V under TFY mode.

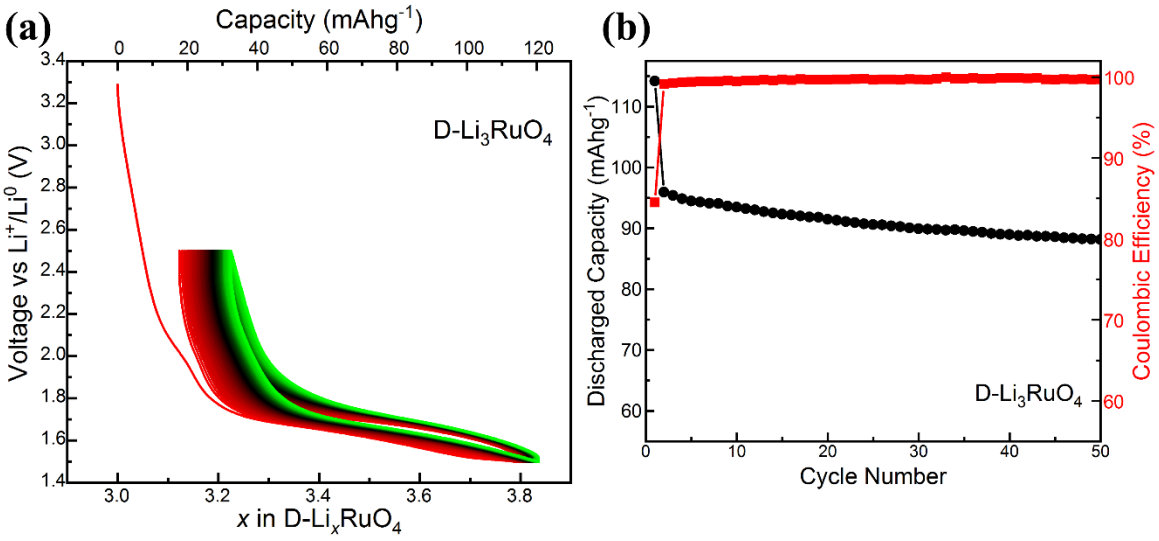

Figure S15. Voltage-composition profile of D-Li_3RuO_4 between 2.5 and 3.9 V; (b) Discharge capacity and coulombic efficiency of D-Li_3RuO_4 as a function of the cycle number.

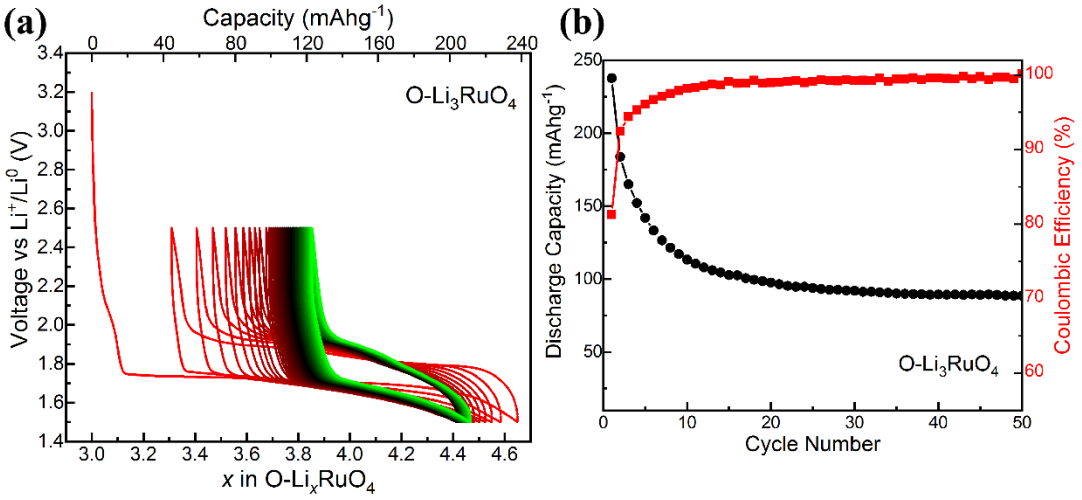

Figure S16. Voltage-composition profile of O-Li_3RuO_4 between 2.5 and 3.9 V; (b) Discharge capacity and coulombic efficiency of O-Li_3RuO_4 as a function of the cycle number.

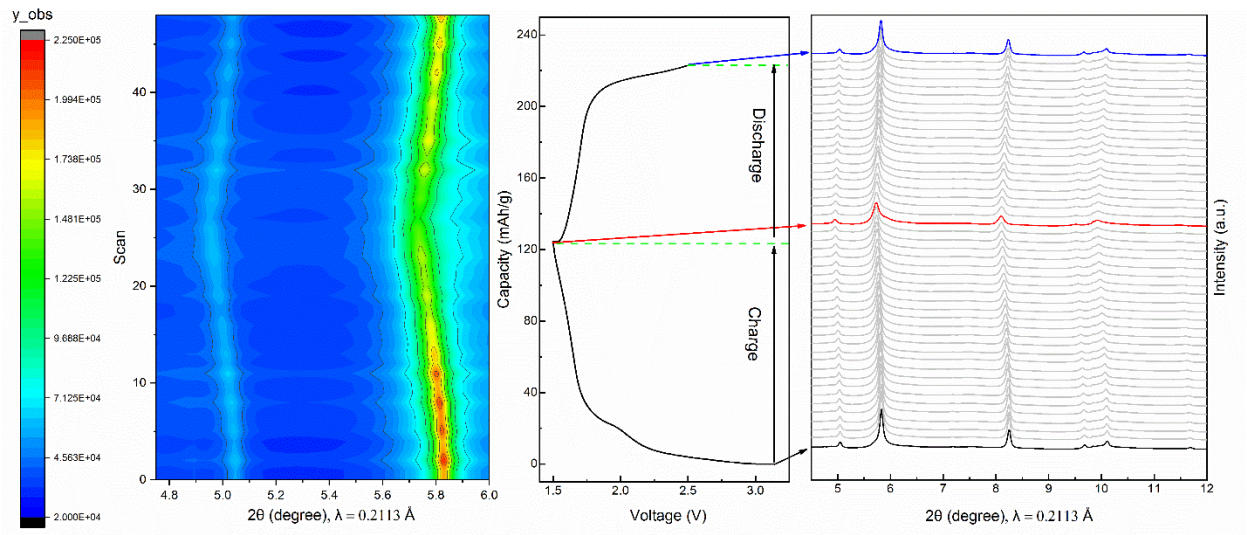

Figure S17. *Operando* SXRD patterns in the first cycle of a D-Li_3RuO_4/Li half-cell at a rate of C/20. The left and middle panels show the contour plot and the corresponding galvanostatic curve between 1.5 and 2.5 V. Black, red and blue patterns represent the pristine, the fully discharged and the fully charged state, respectively.

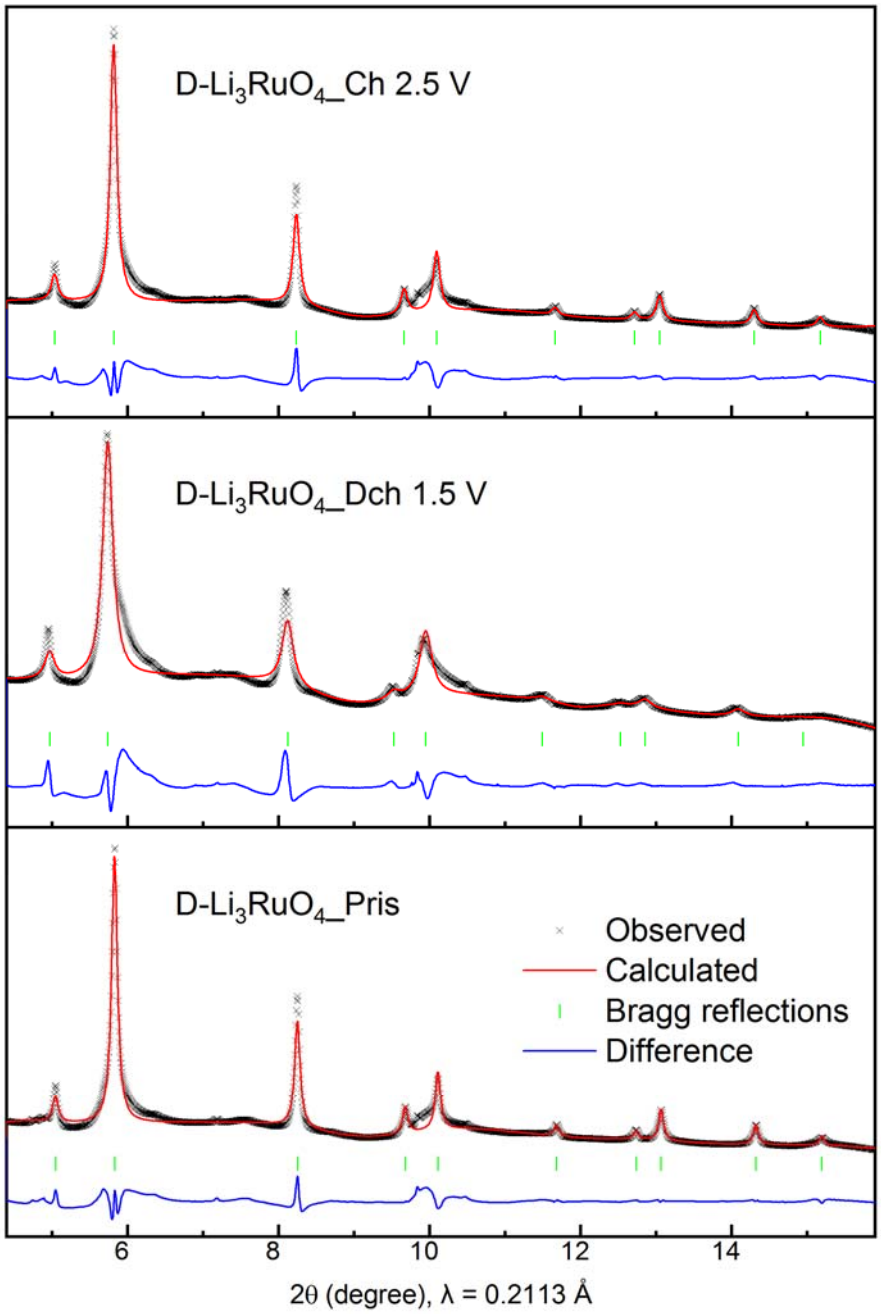

Figure S18. Pawley refinements of SXRD patterns of D-Li_3RuO_4 at different electrochemical states between 1.5 and 2.5 V.

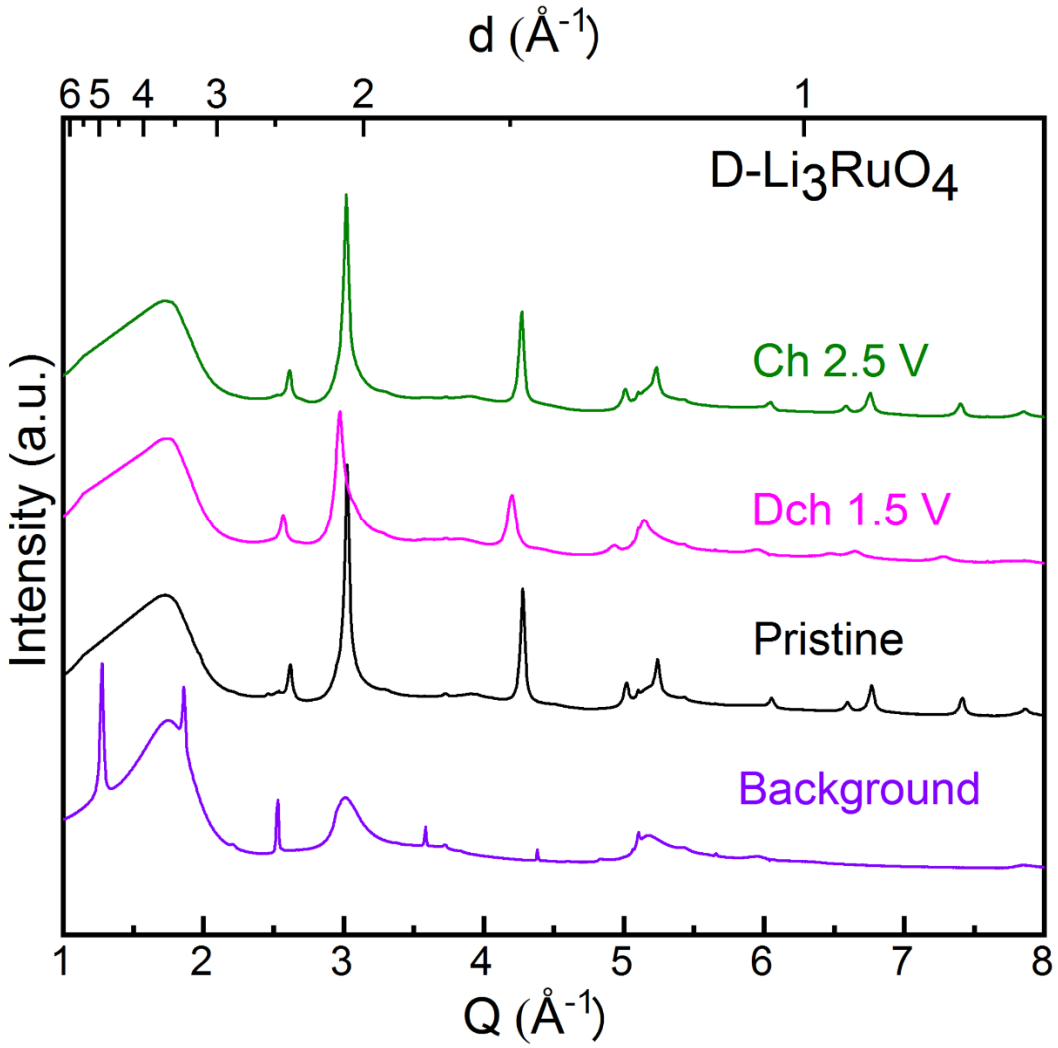

Figure S19. SXRD patterns of D-Li_3RuO_4 at different electrochemical states, compared to a blank pattern of the *operando* cell.

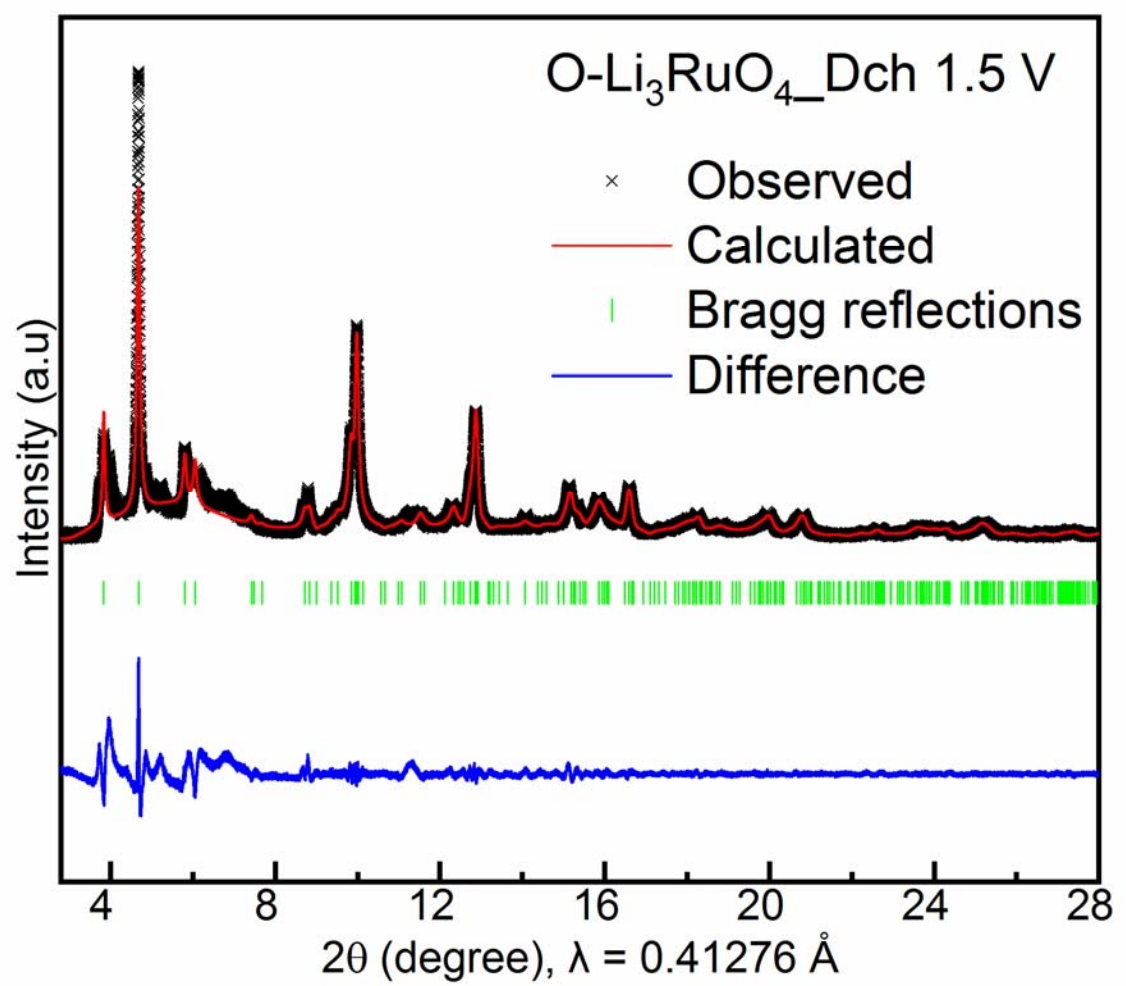

Figure S20. Rietveld refinement of SXRD pattern of $Li_{4.6}RuO_4$. The black crosses and red solid line represent the observed and calculated patterns. The green vertical tick bars denote the Bragg reflections. The blue continuous line is the difference between calculation and observation.

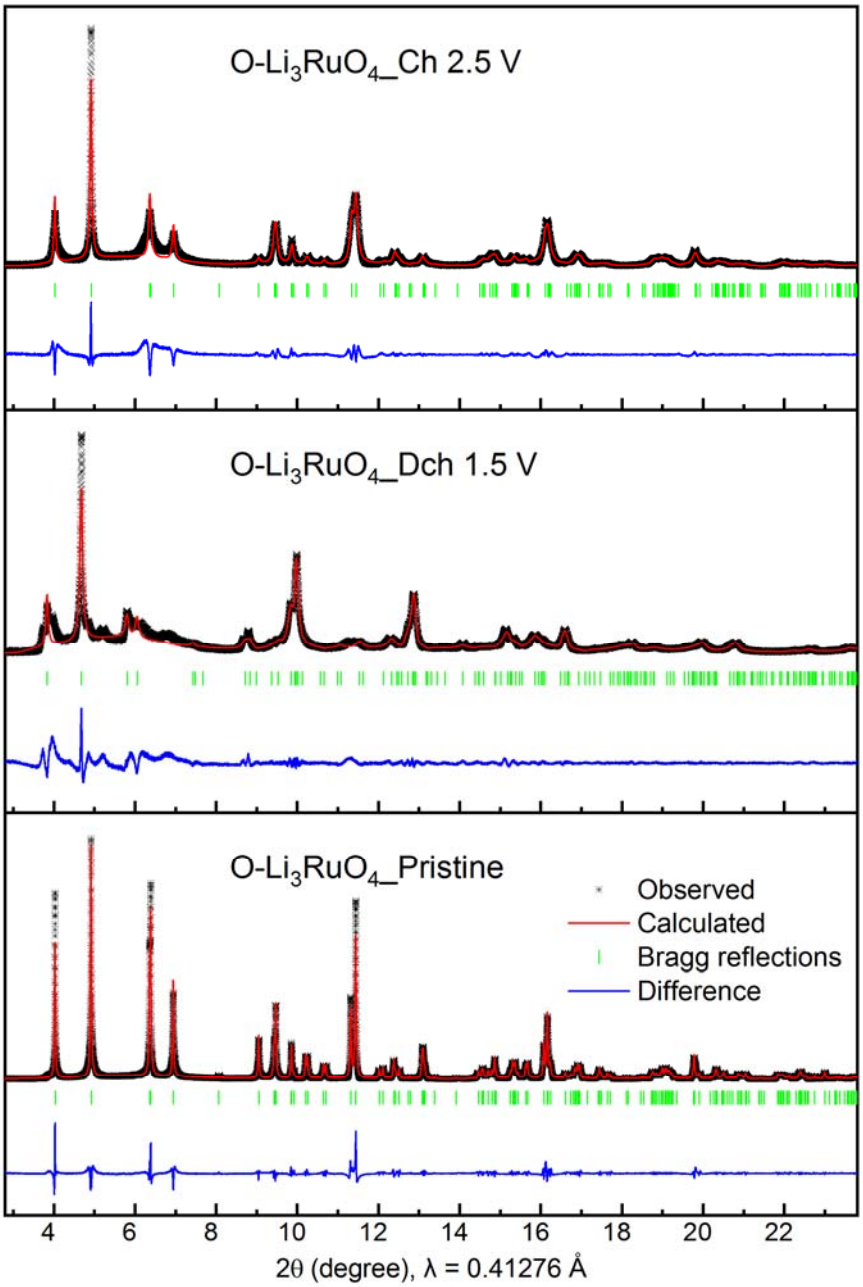

Figure S21. Pawley refinements of SXRD patterns of O-Li_3RuO_4 at different electrochemical states between 1.5 and 2.5 V.

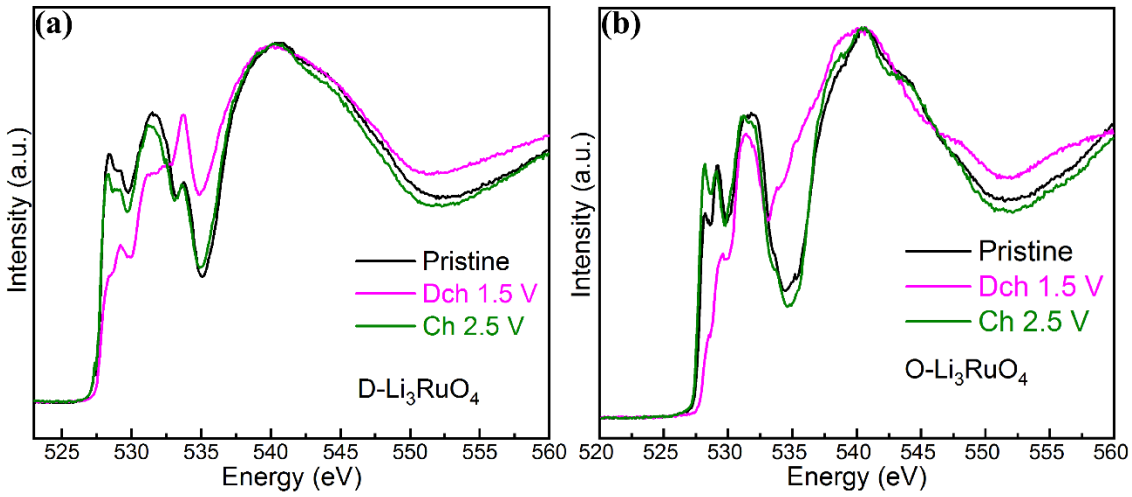

Figure S22. Overlaid *ex situ* O K-edge XAS spectra of (a) D- and (b) O-Li_3RuO_4 measured at different electrochemical states between 1.5 and 2.5 V.

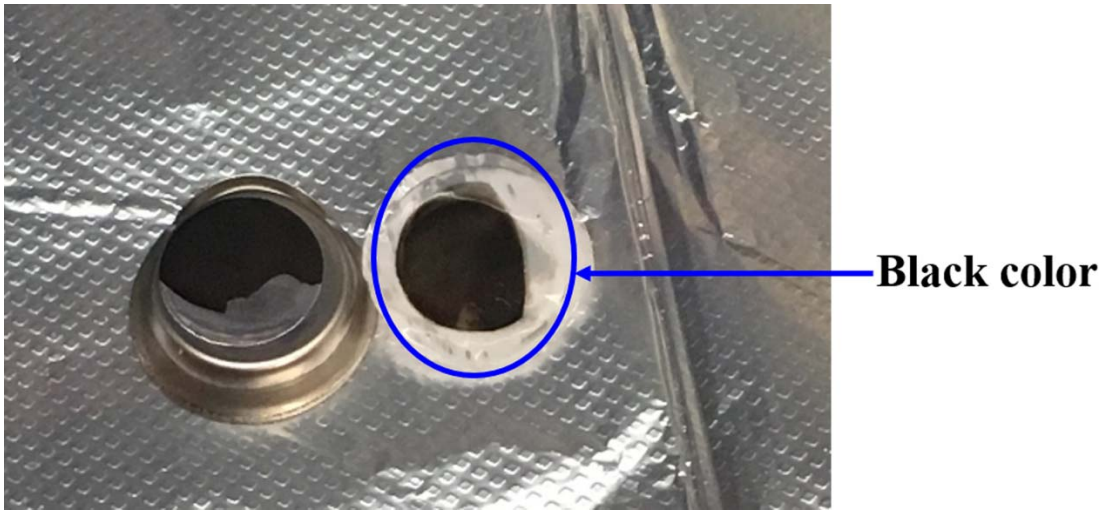

Figure S23. Image of a coin cell after the removal of 0.5 mol of Li from per mol of O-Li_3RuO_4. Clear black color can be observed on the otherwise white separator.

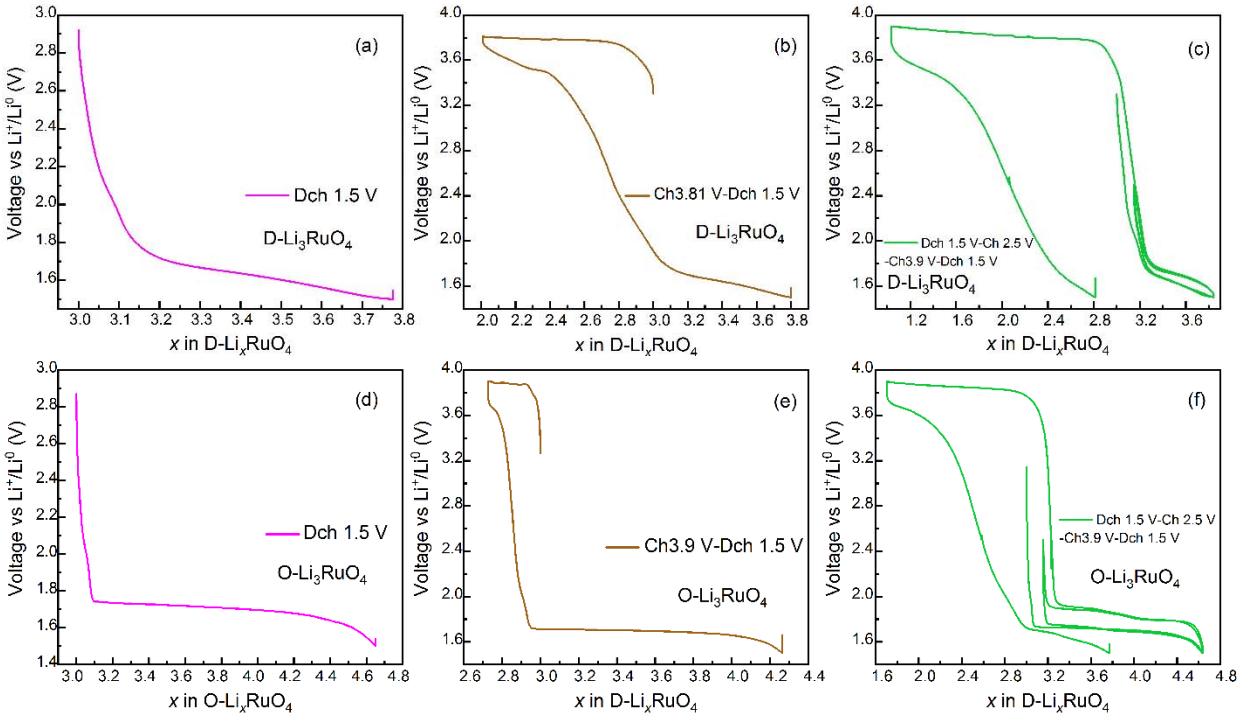

Figure S24. Voltage-composition profiles of (a-c) D-Li_3RuO_4 and (d-f) O-Li_3RuO_4 at different states of charge. (a) and (d) directly discharged to 1.5 V, (b) charged to 3.81 V and discharged to 1.5 V, (e) charged to 3.9 V and discharged to 1.5 V, (c) and (f) cycled between 1.5 and 2.5 V and then charged to 3.9 V and discharged to 1.5.

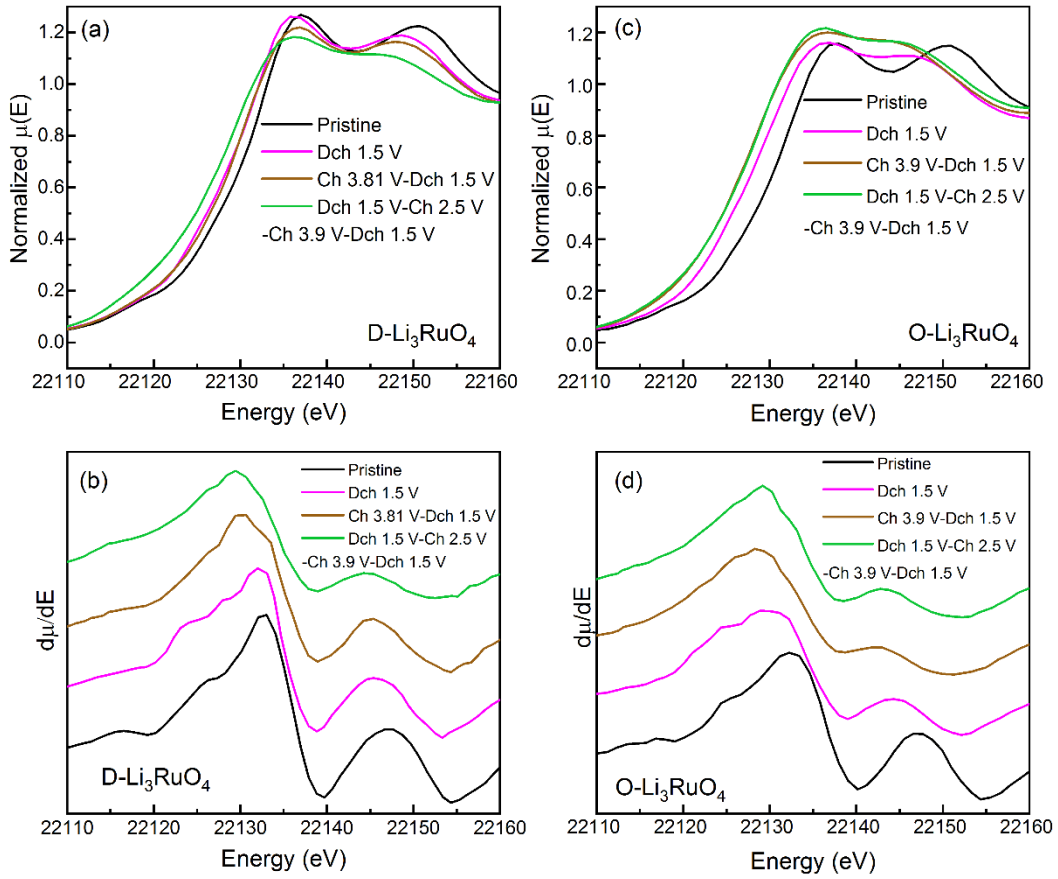

Figure S25. *Ex situ* Ru K-edge XANES spectra of (a) D-Li_3RuO_4 and (c) O-Li_3RuO_4 electrodes in Figure S24, compared to the pristine state, with the corresponding the first derivative curves in (b) and (d).

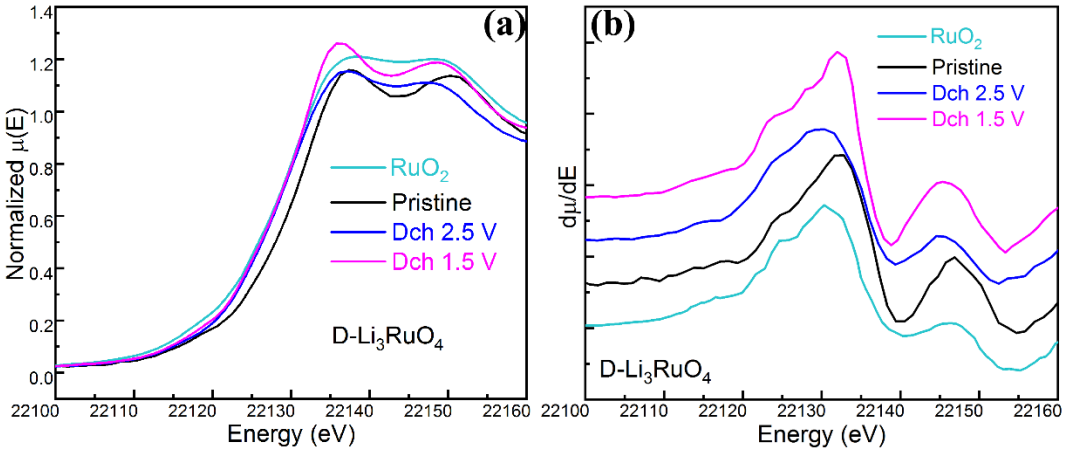

Figure S26. Comparison of the *ex situ* Ru K-edge XANES spectra of D-Li_3RuO_4 in different electrochemical state and (b) corresponding derivative curves.

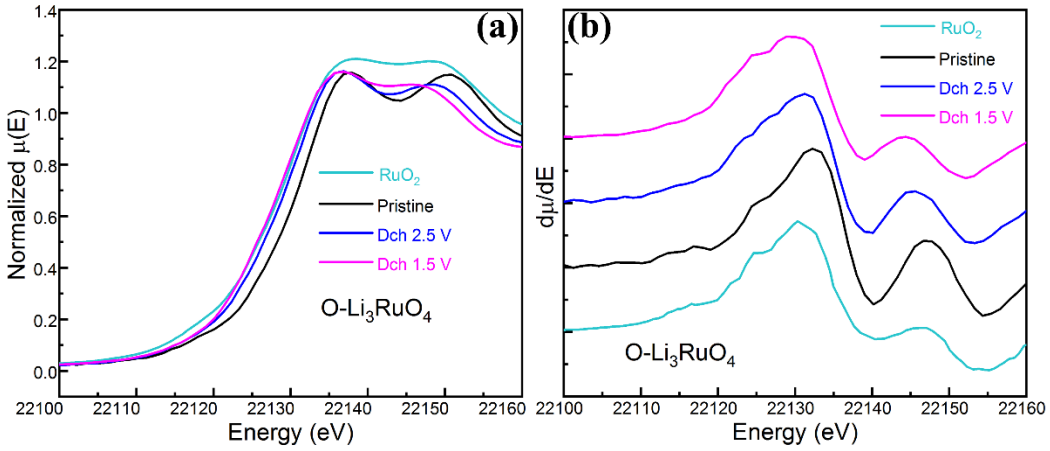

Figure S27. Comparison of the *ex situ* Ru K-edge XANES spectra of O-Li_3RuO_4 in different electrochemical states and (b) corresponding derivative curves.

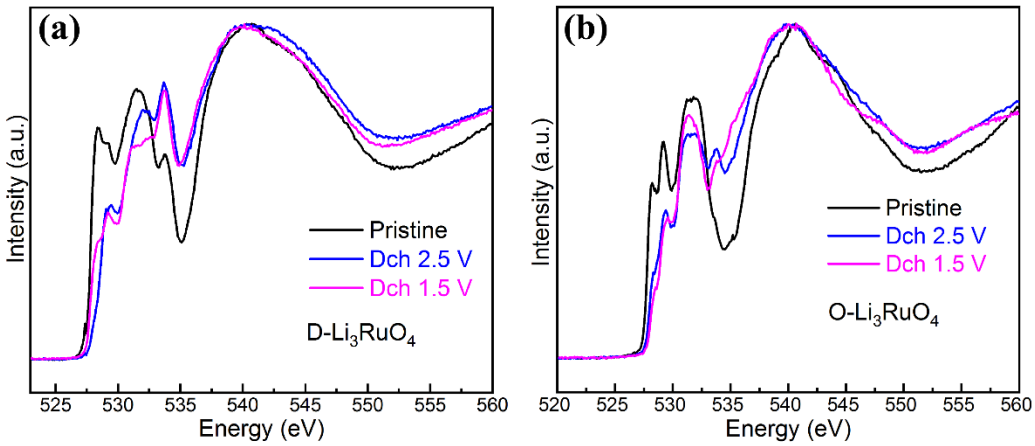

Figure S28. Overlaid *ex situ* O K-edge XAS spectra of (a) D- and (b) O-Li_3RuO_4 measured at different electrochemical states. See text for discussion.

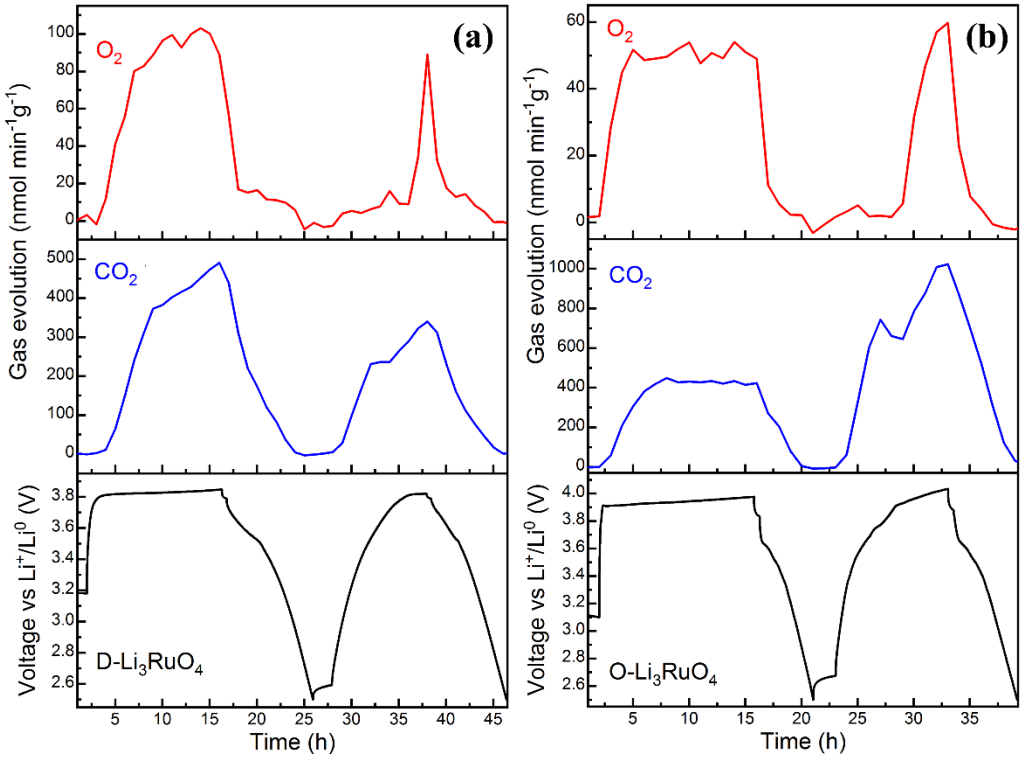

Figure S29. Gas evolution during the first two cycles of D- (black line) and O- (red line) Li_3RuO_4 measured by *operando* DEMS. The voltage profiles are shown in the bottom panels.

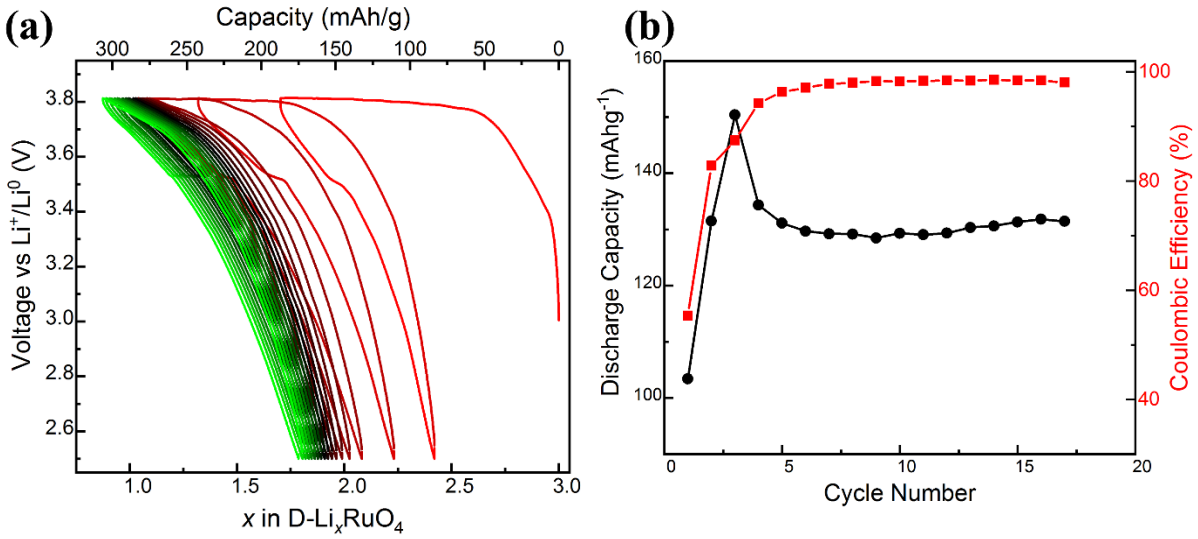

Figure S30. (a) Evolution of the voltage-composition profile upon cycling of a D-Li_3RuO_4 electrode, when the first charge capacity was limited to 1.25 mol of Li extracted; (b) Discharge capacity and coulombic efficiency as a function of the cycle number.

SUPPLEMENTARY TABLES

Table S1 Crystallographic parameters and reliability factors extracted from the joint Rietveld refinement of SXRD and NPD for (a) D- and (b) O-Li_3RuO_4.

(a) D-Li_3RuO_4						
Space group: $Fm\bar{3}m$; a = b = c = 4.14570(8) Å; α = β = γ = 90°; V = 71.252(4) $Å^3$						
Atom	Wyckoff position	x	y	z	U_{iso} ($Å^2$)	Occupancy
O	4b	0.5	0.5	0.5	0.013	1
Li	4a	0.0	0.0	0.0	0.00966	0.75
Ru	4a	0.0	0.0	0.0	0.00966	0.25
R_{WP} = 8.283%; χ^2 = 1.808						
(b) O-Li_3RuO_4						
Space group: P2/a; a = 5.08609(30) Å; b = 5.86578(5) Å; c = 5.12048(30) Å; β = 110.1506(8)°; V = 143.4134(25) $Å^3$						
Atom	Wyckoff position	x	y	z	Uiso ($Å^2$)	Occupancy
O1	4g	0.01853(11)	0.63695(12)	0.75681(10)	0.01058(7)	1
O2	4g	0.50395(12)	0.11326(11)	0.222587(9)	0.01058	1
Li1	2e	0.7500	0.6195(6)	0.0000	0.0251(3)	1
Li2	2f	0.7500	0.9064(6)	0.5000	0.0251	1
Li3	2f	0.7500	0.4209(5)	0.5000	0.0251	1
Ru4	2e	0.2500	0.85995(12)	0.0000	0.06578(22)	1
R_{WP} = 12.316%; χ^2 = 2.869						

Table S2 Selected bond lengths (Å) O-Li_3RuO_4 at 298 K

Bonds	Distance (Å)
Li1-O1	2.1443(6)
Li1-O1	2.1443(6)
Li1-O1	2.0469(25)
Li1-O1	2.0469(25)
Li1-O2	2.1056(26)
Li1-O2	2.1056(26)
Li2-O1	2.2034(24)
Li2-O1	2.2034(24)
Li2-O2	1.9490(20)
Li2-O2	1.9490(20)
Li2-O2	2.2138(6)
Li2-O2	2.2138(6)
Li3-O1	1.9906(19)
Li3-O1	1.9906(19)
Li3-O1	2.0729(7)
Li3-O1	2.0729(7)
Li3-O2	2.3629(23)
Li3-O2	2.3629(23)
Ru4-O1	1.9072(7)
Ru4-O1	1.9072(7)
Ru4-O2	2.0456(8)
Ru4-O2	2.0456(8)
Ru4-O2	1.9813(6)
Ru4-O2	1.9813(6)

Table S3. Delivered capacities and the corresponding O_2 and CO_2 evolution during the *operando* DEMS measurement.

First cycle				
	D-Li_3RuO_4		O-Li_3RuO_4	
	Charge	Discharge	Charge	Discharge
Capacity ($mAhg^{-1}$)	205.4	131.1	200.3	69.1
Evolved O_2 (μmol)	0.42		0.30	
Evoved CO_2 (μmol)	1.98		2.43	
Second cycle				
	D-Li_3RuO_4		O-Li_3RuO_4	
	Charge	Discharge	Charge	Discharge
Capacity ($mAhg^{-1}$)	143.7	114.3	145.3	81.9
Evolved O_2 (μmol)	0.09		0.10	
Evolved CO_2 (μmol)	1.13		3.94	

Table S4. Crystallographic parameters and reliability factors extracted from Rietveld refinement of SXRD of $Li_{4.6}RuO_4$.

$Li_{4.6}RuO_4$						
Space group: P 2/a; a = 5.4354(4) Å; b = 6.1659(4) Å; c = 5.05606(23) Å; β = 90.650(6)°; V = 169.438(15) $Å^3$						
Atom	Wyckoff position	x	y	z	Uiso ($Å^2$)	Occupancy
O1	4g	-0.60433	0.14054	-0.74482	0.0080(8)	1
O2	4g	-0.59751	0.63175	0.75443	0.0080	1
Li3	2e	0.25000	0.898645	0.00000	0.0159	0.292
Ru4	2e	0.25000	0.898645	0.00000	0.0159(5)	0.708
Li5	2f	0.7500	0.63450	0.00000	0.0168	0.292
Ru6	2f	0.7500	0.63450	0.00000	0.0168(4)	0.708
Li7	4g	0.44111	0.09520	-0.32889	0.001	1
Li8	4g	0.47553	0.62858	-0.33087	0.001	1
R_{WP} = 10.817%; χ^2 = 2.11						

BIBLIOGRAPHY

1. Toby, B. H.; Von Dreele, R. B., GSAS-II: the genesis of a modern open-source all purpose crystallography software package. *J. Appl. Cryst.* **2013,** 46, 544-549.

2. Borkiewicz, O. J.; Shyam, B.; Wiaderek, K. M.; Kurtz, C.; Chupas, P. J.; Chapman, K. W., The AMPIX electrochemical cell: a versatile apparatus for in situ X-ray scattering and spectroscopic measurements. *J. Appl. Cryst.* **2012,** 45, 1261-1269.

3. Ravel, B.; Newville, M., ATHENA, ARTEMIS, HEPHAESTUS: data analysis for X-ray absorption spectroscopy using IFEFFIT. *J. Synchrotron Rad.* **2005,** 12, 537-541.

4. McCloskey, B. D.; Bethune, D. S.; Shelby, R. M.; Girishkumar, G.; Luntz, A. C., Solvents' Critical Role in Nonaqueous Lithium–Oxygen Battery Electrochemistry. *J. Phys. Chem. Lett.* **2011,** 2, 1161-1166.

5. McCloskey, B. D.; Scheffler, R.; Speidel, A.; Bethune, D. S.; Shelby, R. M.; Luntz, A. C., On the Efficacy of Electrocatalysis in Nonaqueous Li– O_2 Batteries. *J. Am. Chem. Soc.* **2011,** 133, 18038-18041.

6. Renfrew, S. E.; McCloskey, B. D., Residual Lithium Carbonate Predominantly Accounts for First Cycle CO_2 and CO Outgassing of Li-Stoichiometric and Li-Rich Layered Transition-Metal Oxides. *J. Am. Chem. Soc.* **2017,** 139, 17853-17860.

7. McCloskey, B. D.; Valery, A.; Luntz, A. C.; Gowda, S. R.; Wallraff, G. M.; Garcia, J. M.; Mori, T.; Krupp, L. E., Combining Accurate O_2 and Li_2O_2 Assays to Separate Discharge and Charge Stability Limitations in Nonaqueous Li–O_2 Batteries. *J. Phys. Chem. Lett.* **2013,** 4, 2989-2993.